An Electro-Optic Sensor for Measurement of Intensive DC Electric Field

Jiahong Zhang and Fushen Chen

Abstract—A lithium niobate (LN) integrated electro-optic (EO) sensor incorporated with a rotating shielding electrode has been designed, fabricated and experimentally demonstrated for measurement of intensive direct current (DC) electric field. As only the shielding electrode is rotated, there is no optical fiber rotation connection problem. Experimental results reveal that the sensor can be used to detect the DC electric field from 4 kV/m to 220 kV/m in the time domain, and the linear correlation coefficient of the input/output is 0.9997. The sensor has potential capability to be used for measurement of the intensive DC electric field.

Index Terms—Lithium niobate, integrated EO sensor, EO effect, field-mill, DC electric field measurement.

Fig. 1. The schematic diagram of the sensing system.

I. INTRODUCTION

DIRECT current electric field measurement plays an important role in guiding optimal designing of high voltage direct current (HVDC) transmission lines and converter stations, as well as in studying of weather phenomena such as thunderstorms [1], [2]. The field-mill sensor which consists of a shielding rotor and a sensing plate is firstly developed and used for measurement of the DC electric field [3]. However, the interference of the metallic structure to the original field cannot be ignored. In addition, it is inconvenient in practical applications as both the shielding rotor and the sensing plate must be connected to the earth. To miniaturize the sensor structure and improve the measurement accuracy, the micro-electro-mechanical system (MEMS) based electric field sensor has been developed for both the DC and alternating current (AC) electric field measurement [4]–[6]. Nevertheless, the electrostatic comb driven micro-machined sensor always requires high driving voltage [4], while the thermally driven micro-electrostatic sensor needs more power dissipation [5]. Moreover, since the shielding electrodes would be displaced towards the electric field source, in the presence of large fields, this type of electric field sensor is not suitable [6]. Compared to the above two types of metal electric field sensors, the optical electric field sensor has superiorities including negligible field

disturbance, broad bandwidth, excellent insulation, and good immunity to electromagnetic interference. In 1982, the first optical DC electric field sensor was developed based on the Pockels effect of a bulk LN crystal [7]. However, as the sensing crystal has to be rotated mechanically to eliminate effects of the accumulated surface charges, the concomitant optical alignment problem becomes apparent and the sensor structure is complex. To avoid the fiber rotation connection problem, a LN bulk optic sensor for measurement of DC electric field in space charge environment has been presented [8], [9]. But, a prior knowledge on the space charge is essential and some discrete optical components such as polarizer, collimating lens are required to couple the light beam into the sensing crystal, which results in the practical measurement is difficult to realize. To further miniaturize the sensor structure and avoid the rotation connection problem, the micro structured photonic crystal fibers filled with nematic liquid crystals had been used as a sensing element for electric field measurement [10]. Besides, the fiber Bragg grating (FBG) sensor based on the electric field induced strain on to the FBG using a piezoelectric crystal has been developed for measurement the DC electric field [11], [12]. Recently, the integrated optical waveguide sensors based on Mach-Zehnder interferometer (MZI) with mono-shielding electrode [13], segmented electrode [14] or tapered antenna [15]–[17] have been developed and used to measure the continuous wave (CW) electric field or the broad band pulsed electric field. However, due to the charge accumulation effect of LN crystal, the response decaying rapidly when the sensor is immersed in DC electric field. Therefore, there is no integrated optical waveguide sensor that can be used to measure the DC field directly.

In this paper, based on the basic principle of the electric field-mill, a LN integrated EO sensor incorporated with a micro

rotating shielding electrode has been designed and fabricated for measurement of intensive DC electric field. By rotating the shielding electrode, the DC electric field under measurement is converted into AC electric field between the sensing electrodes. As a result, the light wave travelling through the optical waveguide is modulated by the converted AC electric field. Compared with current field-mill, MEMS and bulk optic sensors, the developed sensor has advantages of compact structure, good electromagnetic immunity (EMI), having no optical fiber rotation connection problem and being suitable for measurement of intensive electric field.

II. SENSOR CONFIGURATION AND FABRICATION

A. Sensing System

The schematic diagram of the sensing system for measurement of the DC electric field is shown in Fig. 1. As can be seen, the output linear polarized light wave from the tunable laser is connected with the integrated EO DC electric field sensor by using the polarization maintaining fiber (PMF). The integrated EO DC electric field sensor is composed of an optical waveguide sensor and a rotating shielding electrode. As the shielding electrode is rotating, the sensing electrode is periodically exposed to an electric field, which results in an induced AC voltage $u(t)$ is generated between the two parallel sensing electrodes. Then an AC electric field $E_{AC}(t) = u(t)/G_{el}$ (G_{el} is gap of the two parallel sensing electrodes) is generated between the two parallel sensing electrodes. Based on the EO effect of the LN crystal, the optical waveguide refractive index will be changed under such electric field, which results in the phase of the light wave travelling in the optical waveguide is changed. Therefore, the light wave is modulated by the induced AC electric field (optical phase modulation), that is the information of the DC electric field is loaded on the optical carrier. At the receiving end, the output modulated optical signal from the senor is transmitted into the photo detector (PD) by using the single mode fiber (SMF). The DC electric field can be finally acquired according to the output electrical signal from the PD.

As an asymmetric MZI is designed, a static optical phase difference $2\pi n_{eff}\Delta L/\lambda$ is generated (n_{eff}, ΔL are the effective refractive index and length difference of the MZI, λ is the optical wavelength). Therefore, it is possible to set the static phase difference is $\pi/2$ by tuning the optical wavelength λ. As the output optical power of the sensor with no electric field is $1/2P_{in}[1+\cos(2\pi n_{eff}\Delta L/\lambda)]$, when the static optical phase difference $2\pi n_{eff}\Delta L/\lambda$ is set as $\pi/2$, the corresponding output optical power is $1/2P_{in}$. So the wavelength that makes the static output optical power become half of the input can be regarded as optimum. Accordingly, the tunable laser is firstly controlled by the microcontroller to finish once wavelength tuning to acquire the two wavelength channel numbers (N_{max}, N_{min}) which corresponds to the maximum and minimum output optical powers respectively. Then, the middle wavelength channel number N_{mid} = ($N_{max}+N_{min}$)/2 is calculated and set to output the optimum wavelength. The more detailed principles of the sensor operation point control technique have been presented in the previous work [17].
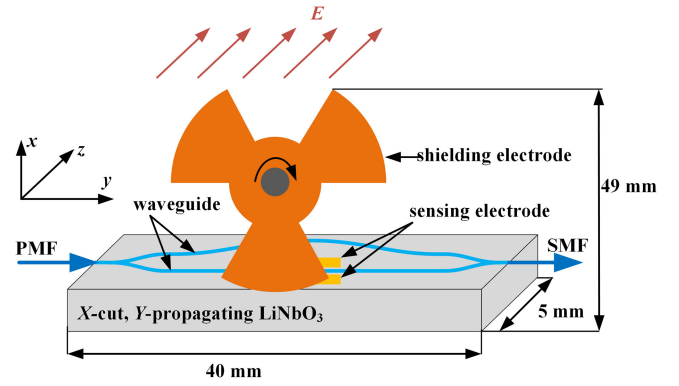

Fig. 2.   Schematic diagram of the integrated EO DC electric field sensor.

B. Operation Principles

The configuration of the designed integrated EO DC electric field sensor is shown in Fig. 2.

As can be seen from Fig. 2, the proposed integrated EO DC electric field sensor is composed of an integrated optical waveguide MZI, two parallel sensing electrodes, a shielding electrode and a micro DC motor. The shielding electrode has three fan-shaped metal plates which is connected with the shaft of the motor. When the motor rotates at speed of n revolutions per minute (RPM), the shielding electrode rotates at speed of n RPM as well, which results the sensing electrode being exposed to the DC electric field at a period of $60/3n$. Based on the basic principles of the field-mill DC electric field sensor [3], the induced charges $Q(t)$ on the sensing electrode is given by

$$Q(t) = \varepsilon_0 ES(t) = \varepsilon_0 ENS_0\left[1 - \cos(N\omega t)\right] \quad (1)$$

where, ε_0 is the dielectric constant in vacuum, E is the DC electric field under measurement, $S(t)$ is the surface area of the sensing electrode exposed to the electric field, S_0 is the surface area of each lobe, N is the number of lobes in the shielding electrode, and ω is the angular velocity of the sensing electrode. Therefore, an induced AC electric field $E_{AC}(t)$ can be described as

$$E_{AC}(t) = \frac{Q(t)}{C_{el}G_{el}} \quad (2)$$

where, G_{el} and C_{el} are the gap and capacitance between the two sensing electrodes. If the transfer function between the DC and AC electric field is $T(t) = \varepsilon_0 NS_0[1-\cos(N\omega t)]/G_{el}C_{el}$, (2) can be simplified as

$$E_{AC}(t) = T(t)E \quad (3)$$

Based on the Pockels effect of the LN crystal, the phase shift of the light wave travelling through the optical waveguide can then be written as [17]

$$\varphi(E) = \frac{\pi n_{eff}^3 \gamma_{33} L_{el}\Gamma T(t)E}{\lambda} \quad (4)$$

where, λ is the input optical wavelength, n_{eff} is the effective refractive index of the optical waveguide, γ_{33} is the EO coefficient, L_{el} is length of the electrode, and Γ is the overlap factor between the optical field and electrical field. When $\varphi(E) = \pi$,

the half-wave electric field E_π can be described as [17]

$$E_\pi = \frac{\lambda}{n_{eff}^3 \gamma_{33} L_{el} \Gamma T(t)} \tag{5}$$

Based on the fundamental principles of the integrated EO MZI type intensity modulator [18], the optical phase difference $\pi E/E_\pi$ of the light wave travelling in the two arms of the MZI is converted into the change of optical intensity at the output Y branch based on the two-beam interference effect. Therefore, add the static phase difference φ_0 (operation point), the output optical power of the sensor can then be described as

$$P_{out} = \frac{1}{2}\alpha P_{in}\left\{1 + b\cos\left[\frac{\pi}{E_\pi}E + \varphi_0\right]\right\} \tag{6}$$

where, P_{in} is the input optical power, α is the insertion loss, b is the extinction coefficient. For the proposed sensor, as an asymmetric MZI is used, the static phase difference can be written as [17]

$$\varphi_0 = \frac{2\pi}{\lambda}n_{eff}\Delta L + \Delta\varphi_0 \tag{7}$$

where, $\Delta\varphi_0$ stands for the shift of the static phase difference caused by the fabrication process error or the change of the external environment conditions such as the temperature, humidity and press. However, it is possible to ensure φ_0 is $\pi/2$ by wavelength tuning based on the operation point control technique proposed previously [14].

Therefore, for $\varphi_0 = \pi/2$, under small modulation ($E_{AC}(t)$ is small and caused $\pi E/E_\pi$ is small), (6) can be simplified as

$$P_{out} = \frac{1}{2}\alpha P_{in}\left\{1 - b\sin\left[\frac{\pi}{E_\pi}E\right]\right\} \approx A - Ab\frac{\pi}{E_\pi}E \tag{8}$$

where, $A = 1/2\alpha P_{in}$, then by substituting (5) into (8), the optical output become

$$P_{out} \approx A - BT(t)E \tag{9}$$

where, $B = Abn_{eff}^3\gamma^{33}L_{el}\Gamma/\pi\lambda$, according to (9), the amplitude of the transfer function $T(t)$ has linear relationship with the DC electric field under measurement. As a result, by using a PD to detect the converted AC electric field, the DC electric field can be acquired.

C. Sensor Design and Fabrication

Based on the COMSOL MULLTIPHYSICS, the three dimension model of the sensor has been established. As can be seen from Fig. 3(a), three fan-shaped metal plates with radius of 24 mm and central angle of 60 degree have been designed as the shielding electrode. Two metal plates with length of 25 mm, width of 2 mm and gap of 10 μm have been designed as the sensing electrode. As the arc length of the sector is $8\pi \approx 25.1$ mm, the sensing electrode can be fully shielded when the shielding electrode is rotated. The vertical gap between the shielding electrode and the sensing electrode is 2 mm. Two parallel plate electrodes with distance of 10 cm and area of 250×150 cm^2 have been established to generate intensive uniform DC electric field. With one of the two parallel plate electrodes is connected with high voltage of 10 kV, an intensive DC electric field of 100

(a)

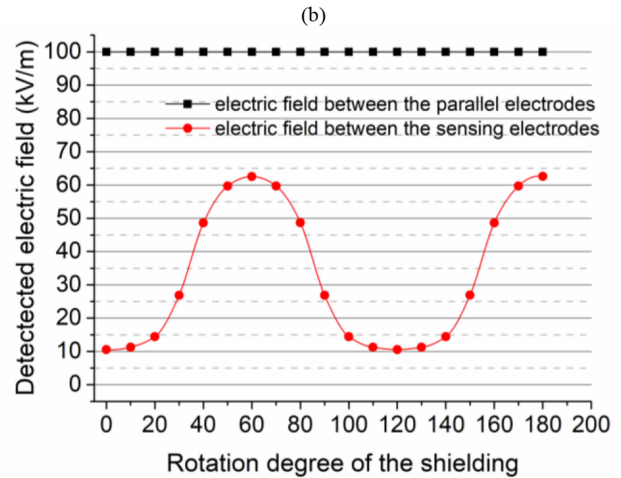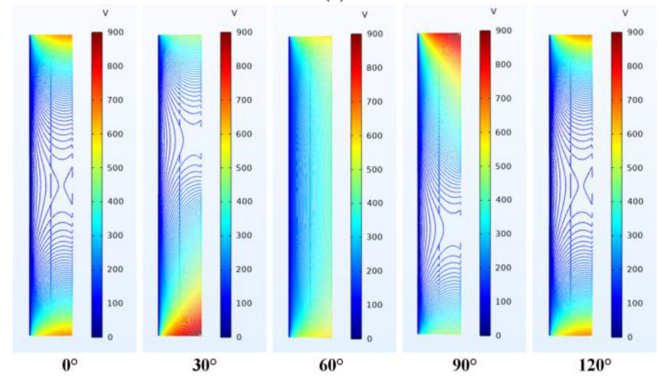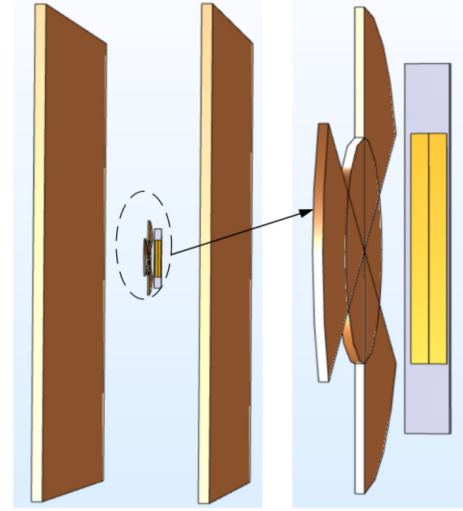0°   30°   60°   90°   120°

(b)

(c)

Fig. 3. Multiphysics simulation (a) three dimensional model, (b) electric potential distribution, and (c) variation of the induced electric field with rotation of the shielding electrode.

kV/m is generated between the two plate electrodes and applied to the sensor.

Assuming when the shielding electrode is rotated at 0°, the sensing electrode is fully shielded by the shielding electrode. By rotating the shielding electrode to different angles, the electric potential distribution on the sensing electrode is simulated.

Fig. 3(b) gives the electric potential distributions when the shielding electrode is rotated at 0°, 30°, 60°, 90° and 120°. As can be seen, when the rotation degree is 0°, the electric potential difference between the two sensing electrodes is very small except for its two ends. With the rotation angel increases, the potential difference increases as well. When the rotation degree is 60°, the sensing electrode is completely exposed to the electric field result in the maximum potential difference. Subsequently, when the shielding electrode rotates to 90° and 120°, the potential go back to that of 30° and 0° respectively. All these results demonstrate that when the shielding electrode is rotated from 0° to 120° the potential difference between the two sensing electrodes changing from the minimum to the maximum and then go back to the minimum.

By using the electric field probe, the induced electric fields are measured with the shielding electrode rotates to different angles. The results are shown in Fig. 3(c). As can be seen, the induced electric fields between the two sensing electrodes varies periodically with rotation of the shielding electrode. As a result, the DC electric field under measurement is converted into AC electric field. In addition, according to Fig. 3(c), the ratio between the applied external DC electric field and the amplitude of the induced AC electric field is calculated as $T \approx 1.6$. By substituting $\lambda = 1550$ nm, $n_{eff} = 2.1$, $\gamma_{33} = 30.8$, $L_{el} = 25$ mm, and $\Gamma = 0.2$ into (5) the amplitude of the halve-wave electric field can be calculated as 679 kV/m. As a result, the maximum detectable electric field of the sensor is approximately equal to $E_\pi/\pi \approx 216$ kV/m.

The integrated optical waveguide sensor is fabricated on x-cut y-propagating LN wafer crystal with dimension of $40 \times 5 \times 1$ mm³. The detailed fabrication processes and technologies of the optical waveguide and metallic electrode have been described in the previous work [14]. To improve mechanical strength and stability of the sensor, the LN wafer has been packaged in an insulated cavity. As shown in Fig. 4(a), the size of the packaged optical waveguide sensor is $55 \times 15 \times 10$ mm³.

Then, a three fan-shaped metal plate with radius of 24 mm and central angle of 60 degree is designed and installed on a micro cylindrical motor (1.5 V/20 mA, $n = 2280$ RPM) to constitute the shielding electrode. The height and radius of the cylindrical motor are 12 mm and 24 mm respectively. An alkaline battery (1.5 V/1600 mAh) is used to drive the motor. Theoretically, the continuous working time of the sensor can up to 80 h. However, the working time can last longer by using a motor with lower power consumption or using a battery with larger capacity. The integrated optical waveguide sensor, the micro DC motor, the shielding electrode, and the battery are all assembled on an insulated substrate to improve the practicability of the sensor. Photograph of the fabricated EO DC electric field sensor is shown in Fig. 4(b). As can be seen, the dimension of the fabricated EO DC electric field sensor is $87 \times 58 \times 17$ mm³.

However, From Fig. 4(b), length and height of the DC electric field sensor are mainly decided by length and width of the integrated optical waveguide sensor respectively, because dimensions of the motor and battery can become smaller. Therefore, to further reduce size of the DC electric field sensor, it is needed to consider further reduce size of the integrated optical waveguide
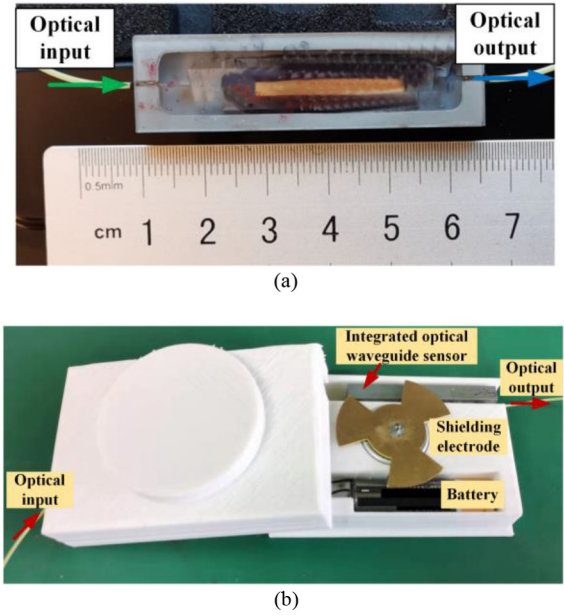

Fig. 4. Photographs of the fabricated devices (a) the integrated optical waveguide sensor, and (b) the EO DC electric field sensor.

sensor. But, to avoid the optical coupling between the two arms of the MZI, width of the optical waveguide senor can hardly be smaller. Therefore, it is possible to reduce the length of the DC electric field sensor by using a shorter sensing electrode to reduce length of the optical waveguide senor. But, there is a trade-off between the sensor sensitivity and length needed to be considered, because a shorter device usually leads to a shorter EO interaction length and a lower sensitivity.

III. EXPERIMENTAL RESULTS

Fig. 5 shows the experimental setup for measurement of the DC electric field by using the fabricated integrated EO DC electric field sensor. As can be seen, the DC high voltage generator with output voltages U from 500 V to 50 kV is connected with the two parallel plate electrodes to generate variable intensive DC electric fields. The dimension of the two plate electrode is $250 \times 150 \times 3$ mm³, and the distance between them is $d = 20$ cm. Hence the uniform DC electric fields ($E = U/d$) from 1 kV/m to 250 kV/m are generated between the two parallel plate electrodes. The sensor is immersed in the DC electric field and its input is connected with the output of the linear polarized tunable laser by using the PMF. To improve the linear characteristic, the operation point of the sensor is adjusted approximately equal to $\pi/2$ by tuning wavelength of the tunable laser using the micro-controller (C851F410). The output optical power, spectral line width and channel spacing of the tunable laser are 13 dBm, 5 MHz and 50 GHz respectively. By using the SMF, the output optical signal from the sensor is transmitted to the optical coupler (OC) to split into two parts. One part is connected with the micro-controller as an optical feedback and the other is connected with the PD as the signal light. The -3 dB band width, voltage gain and noise equivalent power (NEP) of
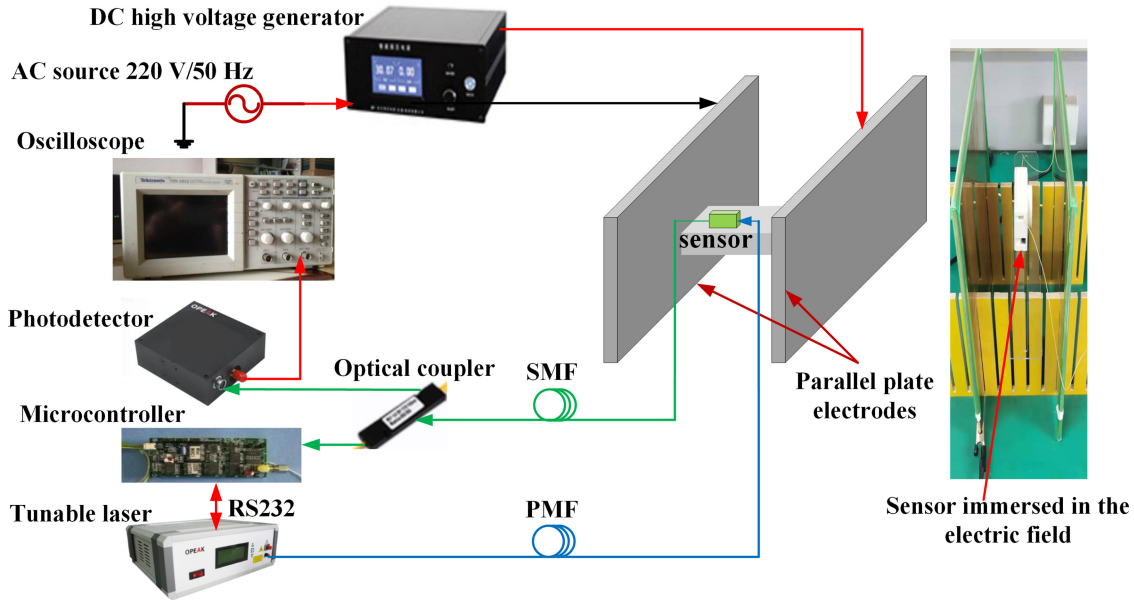
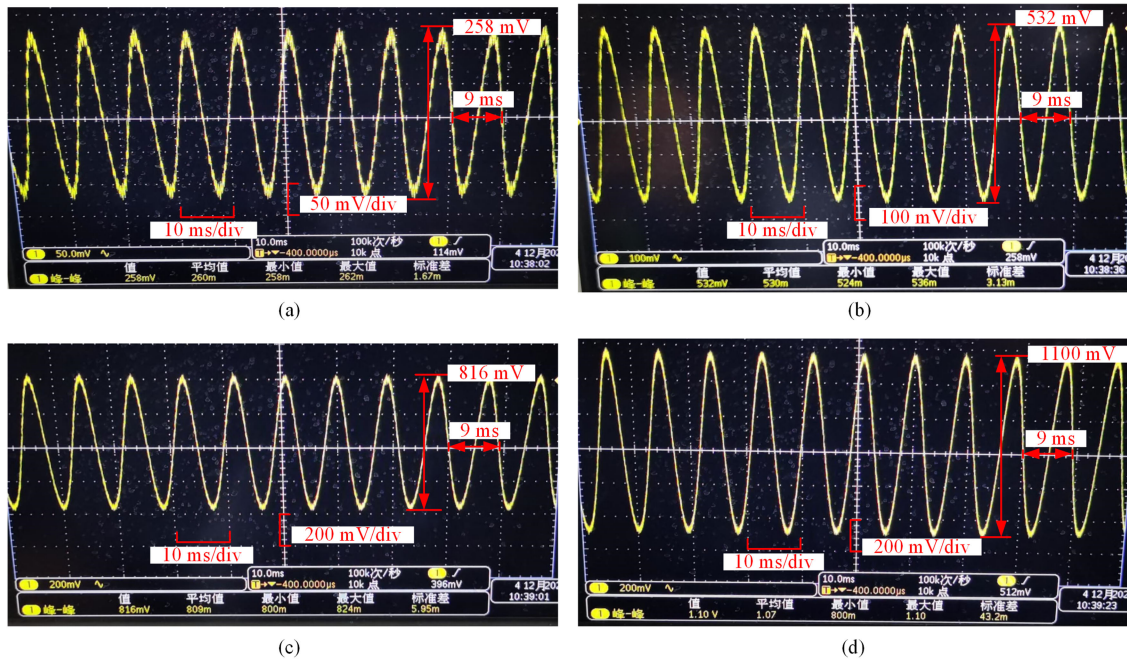Fig. 5. Experimental setup for measurement of the DC electric field.

Fig. 6. The measured AC electric field waveforms (a) $E = 50$ kV/m, (b) $E = 100$ kV/m, (c) $E = 150$ kV/m and (d) $E = 200$ kV/m.

the PD are 200 MHz, 1.4×10^4 V/W, and 10 pW/$\sqrt{\text{Hz}}$, which are sufficient to convert the sensor output optical signal to electrical. Length of both the PMF and SMF is long enough to ensure the personal safety. An oscilloscope with band width of 200 MHz and sampling rate of 2.5 Gb/s (Tektronix MDO3024) is used to extract the output electrical signal from the PD.

In order to show the availability of the DC to AC conversion, the measured waveforms are shown in Fig. 6 when the applied

the DC electric fields are 50 kV/m, 100 kV/m, 150 kV/m and 200 kV/m respectively. As can be seen from Fig. 6(a)-(d), with the applied DC electric fields changed from 50 kV/m to 200 kV/m, the period of the detected AC signals remains at 9 ms, which is consistent with the theoretically calculated result [$T = 1/(3 \times 2280/60) \approx 9$ ms]. However, the amplitudes of the detected AC signals increased linearly with the increase of the applied DC electric fields.
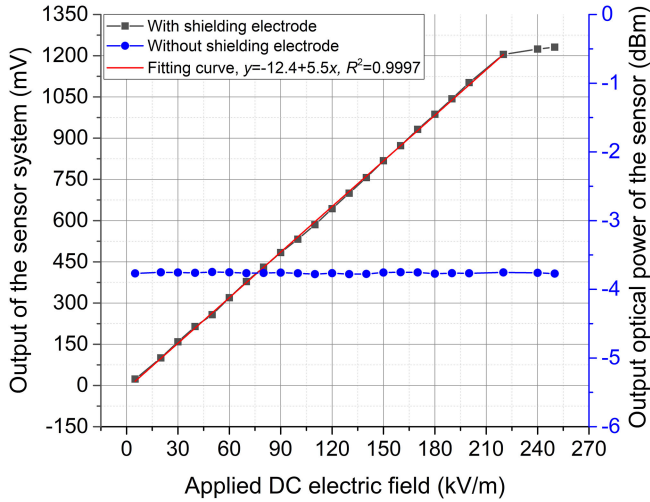
Fig. 7.   Input/output characteristics of the sensor system.

TABLE I
PERFORMANCE COMPARISON

Technology	Measurement range	sensitivity	resolution
This work	4 kV/m-220 kV/m	5.5 mV/(kV/m)	4 kV/m
Field-mill [3]	4 kV/m-80 kV/m	-	4 kV/m
MEMS [4-5]	240 V/m-120 kV/m	4.5 mV/(kV/m)	240 V/m
Optical crystal [7-9]	100 V/m-95 kV/m	5.0 mV/(kV/m)	100 V/m
FBG [11-12]	1 kV/m-1000 kV/m	0.45 pm/(kV/m)	2 kV/m

In addition, the input/output characteristic of the sensor system has been measured with and without the rotating shielding electrode when the applied DC electric fields varied from 5 kV/m to 250 kV/m. Consider the DC output of the sensor system will be filtered out by the PD, the sensor output optical power has been measured directly on condition of without the rotating shielding electrode. The results are shown in Fig. 7. As can be seen, the sensor output optical power remains almost constant without the rotating shielding electrode while output of the sensor system shows good linear characteristics with the rotating shielding electrode, which demonstrates the effectiveness of the method. The linear fitting curve ($y = 5.5x$-12.4) with correlation coefficient of 0.9997 is used to represent the relationship of the sensor input and output. Moreover, consider the noise floor of the sensor system is 10 mV, the minimum detectable electric field of the sensor is approximately equal to 4 kV/m on condition of the signal to noise to ratio (SNR) is 6 dB.

Furthermore, the quantitative comparison with the previous works are shown in Table I. As indicated in Table I, in comparison with the field mill, the MEMS and the optical crystal sensor, the proposed sensor has certain advantage in measurement range. However, the FBG based senor has better superiority in both measurement range and resolution. But as the temperature induced strain is superimposed on the strain induced by the electric field under measurement, which affects the measured results.

Moreover, the root mean square (RMS) error E_{RMS} between the measurement data and the theoretical value is defined as

$$E_{RMS} = \sqrt{\frac{1}{n} \sum_{i=1}^{n} \left(E_{M,i} - E_{T,i}\right)^2} \tag{10}$$

where, $E_{M,\ i} = (V_{out,\ i}+12.4)/5.5$ is the measured electric field, $E_{T,\ i} = U/d$ is the theoretical calculation value, $V_{out,\ I}$ is the output voltage of the sensor system and $n = 21$ is the number of measurement point within the linear measurement range. By substituting the measurement data into (6), the root mean square error is calculated as $E_{RMS} = 1.4909$.

IV. CONCLUSION

In summary, an integrated EO sensor for measurement of the DC electric field sensor has been proposed, designed, fabricated and measured. By integrating an optical waveguide sensor with a rotating shielding electrode, the DC electric field under measurement is converted into AC electric field. The sensor has no optical rotating connection problem. Besides, by using optical fiber for signal input and output, the sensor has good immunity to electromagnetic interference. Experiment results demonstrate that the sensor shows good linear characteristic with the DC electric fields varied from 4 kV/m to 220 kV/m. All these results demonstrate that the sensor has potential capability to be used for measurement the intensive DC electric field.

However, for the proposed sensor, because a battery is needed to drive the shielding electrode, the accuracy and sensitivity will be effected by the stabilization and duration of the power supply. Besides, as the sensor contains moving parts (shielding electrode), the noise and mechanical losses are introduced. To achieve continuous and stable power supply, in the future a photovoltaic power converter can be used to substitute the battery. Moreover, as the mechanical loss mainly caused by the friction loss between the shielding electrode and air, by designing a smoother shielding electrode with smaller radius, and by using a motor with higher stability, smaller dimension and lower power consumption, the sensor dimension and mechanical loss can be further reduced.

REFERENCES

[1] A. Fort, M. Mugnaini, and V. Vignoli, "Design, modeling, and test of a system for atmospheric electric field measurement," *IEEE Trans. Instrum. Meas.*, vol. 60, no. 8, pp. 2778–2785, Aug. 2011.

[2] P. S. Maruvada, "Electric field and ion current environment of HV DC transmission lines: Comparison of calculations and measurements," *IEEE Trans. Power Del.*, vol. 27, no. 1, pp. 401–410, Jan. 2012.

[3] P. S. Maruvada, R. D. Dallaire, and R. Pedneault, "Development of field-mill instruments for ground-level and above-ground electric field measurement under HVDC transmission lines," *IEEE Trans. Power App. Syst.*, vol. PAS-102, no. 3, pp. 738–744, Mar. 1983.

[4] C. Peng *et al.*, "Design and testing of a micromechanical resonant electrostatic field sensor," *J. Micromechanics Microengineering*, vol. 16, pp. 914–919, Mar. 2006.

[5] X. Chen *et al.*, "Thermally driven micro-electrostatic field meter," *Sensors Actuators A: Phys.*, vol. 132, no. 2, pp. 677–682, Nov. 2006.

[6] S. Ghionea, G. Smith, J. Pulskamp, S. Bedair, C. Meyer, and D. Hull, "MEMS electric-field sensor with lead zirconate titanate (PZT)-actuated electrodes," in *Proc. IEEE Sensors*, Baltimore MD, USA, Nov. 2013, pp. 1–4.

[7] K. Hidaka and H. Fujita, "A new method of electric field measurements in corona discharge using pockel's device," *J. Appl. Phys.*, vol. 53, no. 9, pp. 5999–6003, Aug. 1982.

[8] F. Cecelja, M. Bordovsky, and W. Balachandran, "Lithium niobate sensor for measurement of DC electric fields," *IEEE Trans. Instrum. Meas.*, vol. 50, no. 2, pp. 465–469, Apr. 2001.

[9] F. Cecelja, M. Bordovsky, and W. Balachandran, "Electro-optic sensor for measurement of DC fields in the presence of space charge," *IEEE Trans. Instrum. Meas.*, vol. 51, no. 2, pp. 282–286, Apr. 2002.

[10] T. R. Wolinski *et al.*, "Photonic liquid crystal fiber as a sensing element for electric field measurement," in *Proc. IEEE Instrum. Meas. Technol. Conf.*, Warsaw, Poland, May 2007, pp. 1–4.

[11] H. Anirudh, M. V. Reddy, R. L. N. Sai Prasad, and B. Sobha, "DC electric field measurement using FBG sensor," in *Proc. Workshop Recent Adv. Photon.*, Bangalore, India, Dec. 2015, pp. 1–4.

[12] F. Marignetti *et al.*, "Fiber Bragg grating sensor for electric field measurement in the end windings of high-voltage electric machines," *IEEE Trans. Ind. Electron.*, vol. 63, no. 5, pp. 2796–2802, May 2016.

[13] R. Zeng, J. Yu, B. Wang, B. Niu, and Y. Hua, "Study of an integrated optical sensor with mono-shielding electrode for intense transient *E*-field measurement," *Measurement*, vol. 50, pp. 356–362, Jan. 2014.

[14] J. Zhang, L. Yang, and Y. Li, "Non-invasive measurement of intensive power-frequency electric field using a LiNbO$_3$ integrated optical waveguide sensor," *IET Sci., Meas. Technol.*, vol. 15, pp. 101–108, Jan. 2021.

[15] J. Zhang, H. Lu, and Z. Zhao, "Study of an integrated optical waveguide sensor with a tapered antenna for measurement of intense pulsed electric field," *Optik*, vol. 218, pp. 1648371–1648377, Sep. 2020.

[16] C. Chung *et al.*, "Silicon-based hybrid integrated photonic chip for *ku* band electromagnetic wave sensing," *J. Lightw. Technol.*, vol. 36, no. 9, pp. 1568–1575, May 2018.

[17] J. Zhang, C. Luo, and Z. Zhao, "Design and application of integrated optics sensor for measurement of intense pulsed electric field," *J. Lightw. Technol.*, vol. 37, no. 4, pp. 1440–1448, Feb. 2019.

[18] R. C. Alferness, "Waveguide electrooptic modulators," *IEEE Trans. Microw. Theory Techn.*, vol. MIT-30, no. 8, pp. 1121–1137, Aug. 1982.